


Modelling and Design of a Medium Frequency Transformer for High Power DC-DC Converters

Conference Paper**Author(s):**

Stojadinović, Miloš; Biela, Jürgen 

Publication date:

2018

Permanent link:

<https://doi.org/10.3929/ethz-b-000301702>

Rights / license:

[In Copyright - Non-Commercial Use Permitted](#)

Originally published in:

<https://doi.org/10.23919/IPEC.2018.8507864>

Modelling and Design of a Medium Frequency Transformer for High Power DC-DC Converters

M. Stojadinovic, J. Biela
Power Electronic Systems Laboratory, ETH Zürich
Physikstrasse 3, 8092 Zürich, Switzerland

„This material is posted here with permission of the IEEE. Such permission of the IEEE does not in any way imply IEEE endorsement of any of ETH Zürich’s products or services. Internal or personal use of this material is permitted. However, permission to reprint/republish this material for advertising or promotional purposes or for creating new collective works for resale or redistribution must be obtained from the IEEE by writing to pubs-permission@ieee.org.

By choosing to view this document you agree to all provisions of the copyright laws protecting it.”

Modelling and Design of a Medium Frequency Transformer for High Power DC-DC Converters

Miloš Stojadinović*, Jürgen Biela

Laboratory for High Power Electronic Systems, ETH Zürich, Switzerland

*Email: stojadinovic@hpe.ee.ethz.ch

Abstract—Dual Active Bridge (DAB) converters are an interesting solution for battery interfaces in storage systems for traction applications. Due to the environmental conditions and space limitations, the design of the transformer and cooling system is crucial for achieving a high power density. Therefore in this paper a detailed design of a transformer with integrated liquid cooling structure and high isolation voltage is presented. Analytical models for the design are presented and verified with FEM simulations and measurements on a prototype system.

Keywords—Transformer design, modelling, FEM

I. INTRODUCTION

High power DC-DC converters with galvanic isolation are a key element of many applications, as for example medium voltage DC (MVDC) grids [1]–[4], solid-state transformers and power supplies for traction [5]–[8], or more-electric ships [9]. Another application are battery interfaces used in electric vehicles or traction systems [10], [11]. In fig. 1/table I a possible setup and specifications of such a battery interface for a locomotive are given. The system enables to store recuperated energy during braking, what reduces the total energy consumption and enables reuse of the recuperated energy during the acceleration phase. Additionally, energy stored in the batteries can be used to drive the locomotive on non-electrified tracks without a diesel engine, avoiding CO₂ emissions (e.g. in shunt yards). The considered battery interface is based on a dual active bridge (DAB) converter [12]. The series connection of modules at the medium voltage/secondary side allows to use switching devices with lower voltage ratings for all switches. It also makes the transformer isolation requirements more severe. A high efficiency and high power density is required due

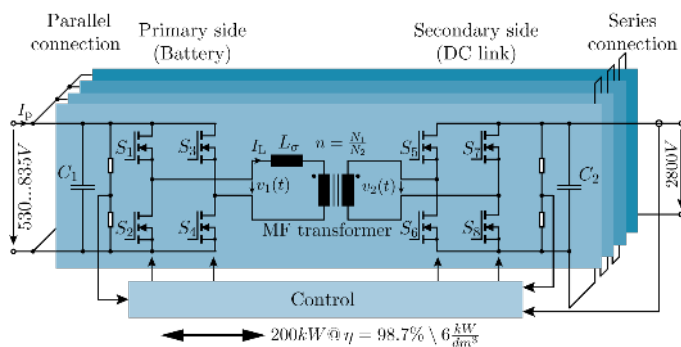


Figure 1. Modular DC-DC converter system based on DAB topology.

Table I. SPECIFICATIONS OF THE BATTERY INTERFACE CONSISTING OF 4 MODULES.

System power (4 modules @ 50 kW)	200 kW
Primary side voltage V_p	530 V..835 V
Nominal primary voltage	710 V
Secondary side voltage V_s	2800 V (4×700 V)
Rated nominal withstand voltage	2.8 kV
Efficiency	>95 %
Power density	>5 kW/dm ³
Ambient temperature	75 °C
Cooling medium temperature	60 °C

to the space limitations in the locomotive. The high power density is achieved by optimising the converter design and by pushing the switching frequency of the semiconductor devices to higher values under ZVS condition. Several examples for high power medium voltage DC-DC converters with galvanic isolation can be found in the literature [1], [4]–[8]. Figure 2 gives a comparison of some of these converter systems in the efficiency/power density plane based on data provided in the literature.

For achieving a high power density, the advanced cooling

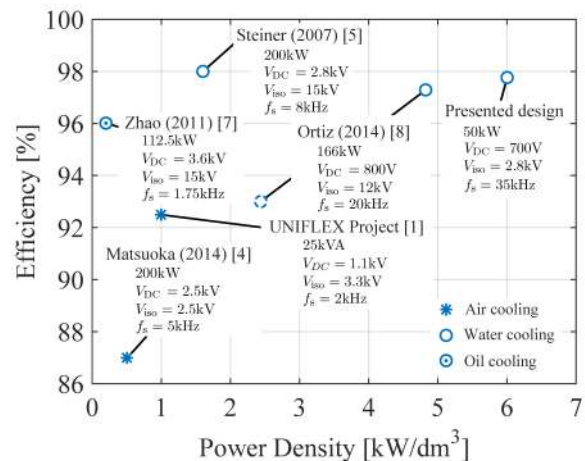


Figure 2. Efficiency / power density comparison of the presented system to the previous state of the art solutions. All the results are given for a single module with full isolation rating of the transformer. For the design presented in [8], both calculated and measured efficiency / power density values are given, where the \bullet represents the measured values. The presented design only shows the calculated efficiency / power density values.

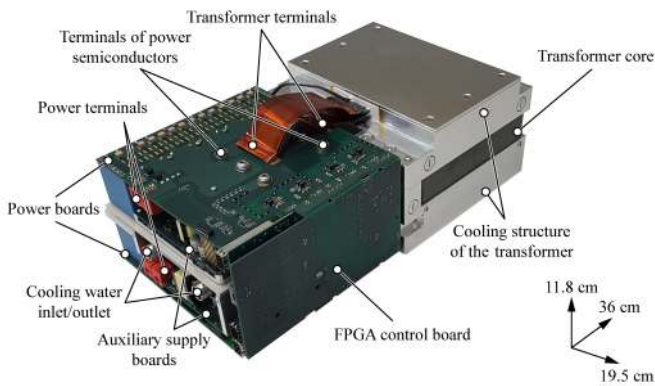


Figure 3. Photo of the single module DAB converter for a modular DC-DC system.

concepts [13] have to be used in transformer. Many designs employ a coaxially wound transformer [5], [14]–[16]. The cooling of such a transformer is usually achieved by using hollow inner conductors [5], [15], [16] through which the de-ionized water is pumped. Another investigated transformer structure is the shell type geometry. The cooling of such a structure can be achieved either with natural or forced convection [17]–[19], using aluminium plates [8] or via heat pipes [20] to conduct the heat from the windings to the core-mounted heat sinks. Due to the switching frequencies in the kHz range, the eddy current losses induced in the structures with aluminium cooling plates lead to higher than predicted temperatures in the transformer. To cope with this issue a thermally conductive coil formers can be used in order to conduct heat from windings to the aluminium heat sink mounted on the transformer core [21]. Unfortunately, the thermal conductivity of such coil formers is considerably lower than for aluminium, which results in larger transformer volumes.

In order to increase the power density, a transformer with integrated liquid cooling is presented in this paper. The cooling system can be operated with tap water, despite the high nominal isolation voltage of $V_{\text{iso}} = 2.8 \text{ kV}$. For designing the integrated cooling structure, analytical thermal models are presented and verified with FEM simulations and measurements. In section II first the short overview of the design procedure is outlined, followed with used models for the transformer design. There, special attention is dedicated to the thermal modelling of the integrated cooling structure with water channels. Results of FEM simulations for different design aspects are given in section III. Finally, experimental measurements on a prototype system are presented in section IV, followed by conclusions.

II. TRANSFORMER DESIGN

The system shown in fig. 1 is used as battery interface in locomotives. Since the secondary side (DC link side) is connected in series, the nominal primary and secondary voltages are almost equal (table I). This enables to use the same

switching devices for both full bridges. For the presented system 1200 V SiC MOSFETs devices are employed. Using SiC MOSFETs under ZVS conditions, enables higher switching frequencies.

In order to determine the parameters for the highest power density, an optimization of the converter modulation scheme and the transformer (fig. 4) is performed for worst case input conditions. The modulation parameters of the DAB converter are the phase shift angle ϕ , clamping interval of the primary side bridge δ_1 , the clamping interval of the secondary side bridge δ_2 and frequency f_s . Illustrative explanation of the modulation parameters is shown in fig. 5. More details about the used modulation schemes and the description of the implementation are given in [22]. The optimization is multi-objective, i.e. both the system volume and the total system losses are minimized.

Starting with the system specifications (table I) at *step 0* in fig. 4, first the converter electrical model for the initial control parameters is derived in *step 1*, giving at the output the voltage/current waveforms and required leakage inductance (L_σ). The voltage/current waveforms (fig. 5) are used to calculate the losses in the switching devices in *step 2*. In *step 3*, the calculated output power P_{out} (defined by the control parameters) is compared to the required power P_{nom} . In the same step, semiconductor losses are calculated and verified to be below the maximum specified losses. If any of the constraints is not fulfilled, the control parameters are changed and the procedure restarts. In *step 4*, the transformer

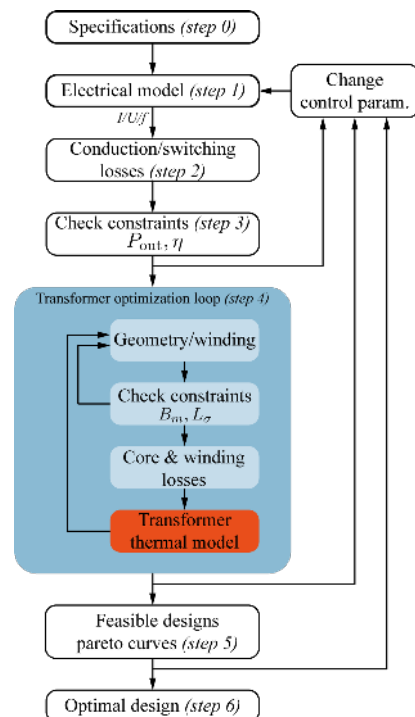


Figure 4. Simplified flow chart for the optimization procedure to find the optimal control variables ϕ , δ_1 , δ_2 , f_s and the optimal transformer design for worst case conditions, by minimizing the DAB converter losses and volume.

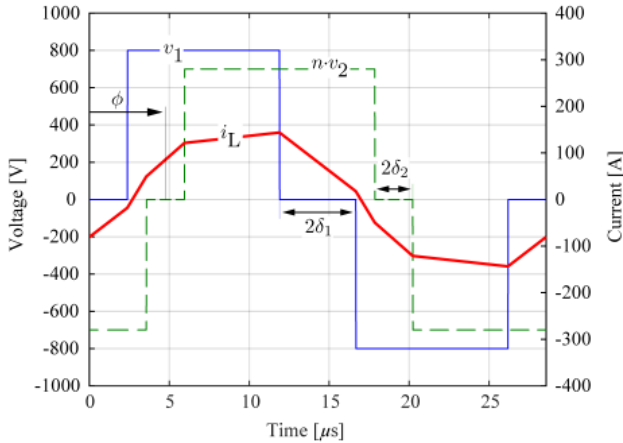


Figure 5. Exemplary voltage and current waveforms at the transformer terminals for a random set of control parameters $[\phi_2, \delta_1, \delta_2]$.

optimization loop is executed which determines a suitable core geometry and winding arrangement that fulfils the following constraints: peak flux density $B_m \leq B_{sat}$, leakage inductance $L = L_{sigma}$ and temperature rise $T \leq T_{max}$. If any of the constraint is not met the calculation restarts with new control parameters. After all the feasible designs are obtained in *step 5*, the optimal design (*step 6*) is chosen at the knee point of the pareto curve.

For the considered system, major challenges are the design of the transformer and the efficient heat removal. In order to improve the heat removal, foil conductors are used for the transformer windings. Using foil only slightly increases the eddy current losses in the windings compared to the litz wire [23], but due to the large copper filling factor and surface area, foil windings are preferred from a thermal and a size point of view. In fig. 6 the CAD drawing of the transformer with integrated cooling system is shown for the specifications given in table I. One of the specifications for the transformer and semiconductor cooling system is to use tap water. Therefore,

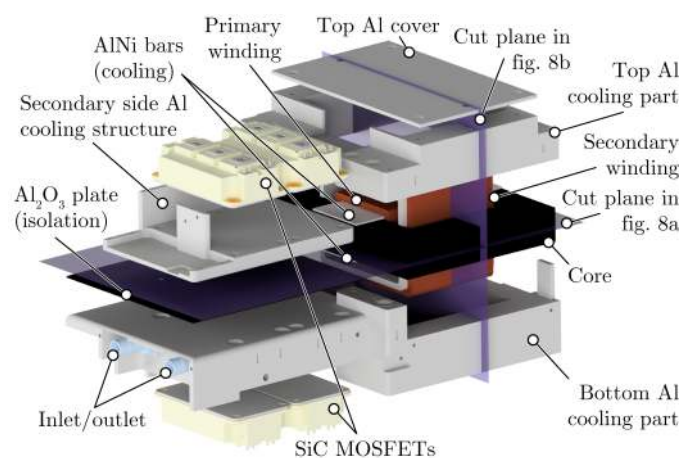


Figure 6. Exploded view CAD drawing of the designed transformer with integrated cooling structure.

the whole liquid cooling structure is at the ground potential. The cooling channels are used for cooling the switches and the transformer. The channel structure can be seen in fig. 10. Because of the high isolation requirement between the transformer windings, the cooling channels are placed only on the outer core legs of the transformer. For removing the heat from the transformer primary winding, first an aluminium bar was considered as a part of the bottom cooling part (fig. 12). The bar is placed between the winding and the transformer middle leg. Due to the induced eddy current losses, the aluminium bar was replaced with an aluminium nitride (AlNi) bar. Aluminium nitride is an electrical isolator which offers high thermal conductivity equivalent to thermal conductivity of aluminium (table II). For cooling the secondary winding and fulfilling the isolation requirement, the transformer is potted using a thermally conductive casting compound *Wepesil VU 4675*, which offers a wide operating temperature range and low hardness.

For isolating the secondary side switches, an aluminium oxide (Al_2O_3) plate is used to separate the secondary side cooling structure, on which the secondary side switches are mounted, and the grounded bottom cooling part. The fixation of the aluminium and Al_2O_3 plate to the main structure is achieved with nylon glass filled bolts. By increasing the outer diameter and rounding the edges of the holes in the aluminium parts (see fig. 7) it is possible to shape the e-field in order to fulfil the given isolation requirements. Table II lists the specifications of the designed medium frequency transformer with important parameters used for thermal modelling.

A. Loss Modelling

In this section, the models used for modelling the transformer core and winding losses are summarized.

Table II. SPECIFICATIONS OF THE MEDIUM FREQUENCY TRANSFORMER.

Element	Material	Thermal Conductivity
Core	N87, N97	4 W/(m K)
Winding isolation	Poly-Pad K10	0.85 W/(m K)
Trafo cold plate	AlNi	> 150 W/(m K)
Switch cold plate	Al_2O_3	20..30 W/(m K)
Potting	Wepesil VU 4675	1.2 W/(m K)
Parameter	Value	
Maximum frequency	35 kHz	
Leakage inductance	26.5 μ H	
Primary turns	20	
Secondary turns	20	
Primary foil winding thickness	100 μ m	
Secondary foil winding thickness	100 μ m	
Primary winding losses	73 W	
Secondary winding losses	150 W	
Core losses N87 (N97)	45 W (37 W)	

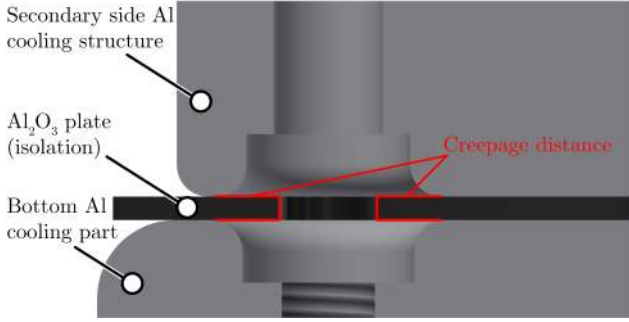


Figure 7. Cut view of the fixation point between bottom cooling part and secondary side cooling structure.

1) *Winding Losses*: Since foil windings are used for the design of the transformer, the method outlined in [24] is used for calculating the skin and proximity effect losses. The method is based on an 1D approximation of the H-field in the windings, which results in the resistance factor expressed in the term of hyperbolic trigonometric functions of the skin penetration depth.

2) *Core Losses*: For calculating the transformer core losses the Improved Generalized Steinmetz Equation (iGSE), presented in [25], is used. This procedure takes the derivative of the flux waveform, as well as the peak-to-peak value of the flux into account in order to calculate the core loss. The method offers good precision with low complexity, which is advantageous for optimization problems.

Care must be taken when using manufacturer loss measurements for core materials. These measurements are usually performed on small toroidal cores and the losses might be significantly lower (2-3x) compared to the losses in the cores with different shapes (e.g. large E-/U-core). It is advisable to compare the losses of the actual used core, usually given just for a single frequency and flux point, to the same point on the loss curves in the material datasheet, and scale the curves accordingly. The core materials which are used and compared during the design procedure are *EPCOS N87* and *EPCOS N97* (table II).

B. Leakage Inductance Modelling

The winding height in transformer design with relatively high isolation requirements is typically smaller than the core window height. In order to calculate the leakage inductance in such design, a formula that employs the *Rogowski* coefficient can be used [26]

$$L_{\sigma} = \mu_0 N_p^2 \frac{\pi D_{\text{mean}} w_L}{\sqrt{h_{\text{cuP}} \cdot h_{\text{cuS}}}} k_{\sigma} \quad (1)$$

where N_p is the number of primary turns, D_{mean} is the mean diameter of the reduced leakage channel, w_L is the width of the reduced leakage channel, h_{cuP} is the primary winding height, h_{cuS} is the secondary winding height, and k_{σ} is the *Rogowski* coefficient. A simplified illustration of the transformer winding structure is depicted in fig. 8. The expressions for calculating the required parameters in the leakage inductance formula have

been adapted for taking into account the non-circular shape of the windings

$$w_L = \frac{d_P + d_S}{3} + d_L \quad (2)$$

$$k_{\sigma} \approx 1 - \frac{d_P + d_S + d_L}{\pi \sqrt{h_{\text{cuP}} \cdot h_{\text{cuS}}}} \quad (3)$$

$$D_{\text{mean}} = D + d_P + d_L + d_S - \frac{d_S - d_S}{2} \frac{d_P + d_S + 4d_L}{d_P + d_S + 3d_L} \quad (4)$$

where D is the equivalent diameter of the core leg, and can be calculated as

$$D = 2\sqrt{\frac{b_c d_c}{\pi}} \quad (5)$$

The given formulas for leakage inductance calculation are valid for cases where the heights of the primary and secondary winding are approximately the same.

C. Thermal Modelling

The simplified transformer thermal model used in the optimization procedure (fig. 4) is depicted in fig. 9. The full scale model is more detailed, derived in a matrix form with the size 11×11 . It is assumed that the secondary winding bobbin acts as a thermal isolator, and that the primary winding is mainly cooled through the AlNi bar. The picture (fig. 9) is split in two 2D cut planes, each showing a cut view of the transformer with integrated cooling structure (see fig. 6). There also the thermal resistances ($R_{\text{th,r}}$, $R_{\text{th,d}}$) of the water channel are shown. These thermal resistances can be calculated using

$$R_{\text{th,r}} = \frac{0.5 \cdot (w - d)}{bl\lambda_{\text{HS}}} \quad (6)$$

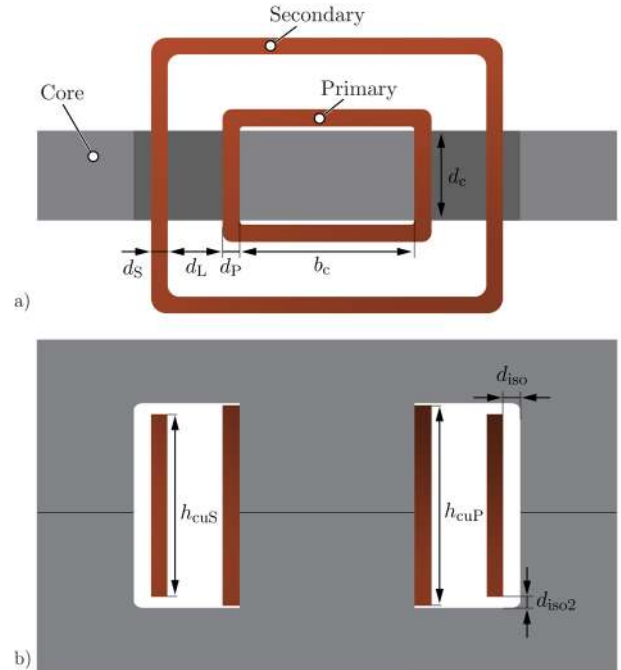


Figure 8. Transformer geometry for calculating leakage inductance.

$$R_{th,d} = \frac{1}{hl\pi d} \quad (7)$$

where w is the width of the heat sink, b is the height of the heat sink, l is the length of the heat sink, d is the channel diameter, and λ_{HS} is the thermal conductivity of heat sink material. Parameter h is the heat transfer coefficient which can be calculated with

$$h = \frac{N_u \lambda_{fluid}}{d} \quad (8)$$

For calculating the heat transfer coefficient, it is necessary to know the *Nusselt* number (N_u). The *Nusselt* number is, in general, a function of the average ducted fluid velocity, duct geometry, and the fluids *Prandtl* number (Pr). The author of [27] has derived an analytical model for the generalized *Nusselt* number ($N_{u,\sqrt{A}}$) that is suitable for the extruded heat sink model with arbitrary cross-section

$$N_{u,\sqrt{A}} = \left[\left(\left\{ C_2 C_3 \left(\frac{f Re_{\sqrt{A}}}{d} \right)^{\frac{1}{3}} \right\}^5 + \left\{ C_1 \left(\frac{f Re_{\sqrt{A}}}{8\sqrt{\pi}} \right) \right\}^5 \right)^{\frac{m}{5}} + \left(C_4 \frac{f(Pr)}{\sqrt{d}} \right)^m \right]^{\frac{1}{m}} \quad (9)$$

with

$$f(Pr) = \frac{0.564}{\left[1 + (1.664 Pr^{1/6})^{9/2} \right]^{2/9}} \quad (10)$$

$$f Re_{\sqrt{A}} = \left[\frac{11.8336 \dot{V}}{l \cdot \nu} + (f Re_{fd})^2 \right]^{1/2} \quad (11)$$

$$f Re_{fd} = \frac{12}{2 \left[1 - \frac{192}{\pi^5} \tanh \frac{\pi}{2} \right]} \quad (12)$$

where \dot{V} is the flow rate in [m^3/s], ν is the kinematic viscosity of the channel fluid, and the parameters C_1, C_2, C_3, C_4 are defined in [27] as

$$C_1 = 3.24 \quad C_2 = \frac{3}{2} \quad C_3 = 0.409 \quad C_4 = 2$$

The blending parameter m is defined by

$$m = 2.27 + 1.65 Pr^{\frac{1}{3}} \quad (13)$$

In order to solve the thermal model of the transformer, additional information on the fluid is required. Due to the multiple parallel pipes, the fluid flow in the different channels is different from the input fluid flow. In order to calculate the velocity of the fluid in the parallel channels, the following expressions [28] are used:

$$\Delta h_{tot} = \Delta h_1 = \Delta h_2 = \dots = \Delta h_i \quad (14)$$

$$\dot{V} = \dot{V}_1 + \dot{V}_2 + \dots + \dot{V}_i \quad (15)$$

where Δh_{tot} is the total head loss of the system, and Δh_i ($i = 1, 2, \dots$) are the head losses in the individual channels. \dot{V} and \dot{V}_i ($i = 1, 2, \dots$) designate the input flow rate and flow rate in the individual channels, respectively. For calculating the head losses in the individual channels, the *Moody* relation

$h_f = f(L/d)(V^2/2g)$ can be used [28], where V is the fluid velocity, L is the channel length, f is the channel friction factor, and g is the gravitational acceleration. Each channel has a quadratic parallel resistance, and the head loss is related to the total flow rate by

$$h_f = \frac{\dot{V}^2}{\left(\sum \sqrt{K_i/f_i} \right)^2} \quad (16)$$

where

$$\dot{V} = V \cdot \frac{\pi^2 d_i}{4} \quad K_i = \frac{\pi^2 g \cdot d_i^5}{8 L_i}$$

In the general case, the channel friction factor f_i is a function of the *Reynolds* number and the roughness ratio. Since the *Reynolds* number varies with the fluid velocity, solving of the set of equations must be done iteratively. In the first step, an arbitrary values of f_i are chosen and with them a first estimate of h_f is calculated. Then, the resulting flow rate estimate $\dot{V}_i \approx (K_i h_f / f_i)^{1/2}$ is obtained for each channel. Using these results, a new *Reynolds* number and a better estimate of f_i is calculated. Usually, a few iteration steps are sufficient to obtain a satisfactory solution. When the flow in the channel is laminar, a simple expression for f , known as *Darcy* friction

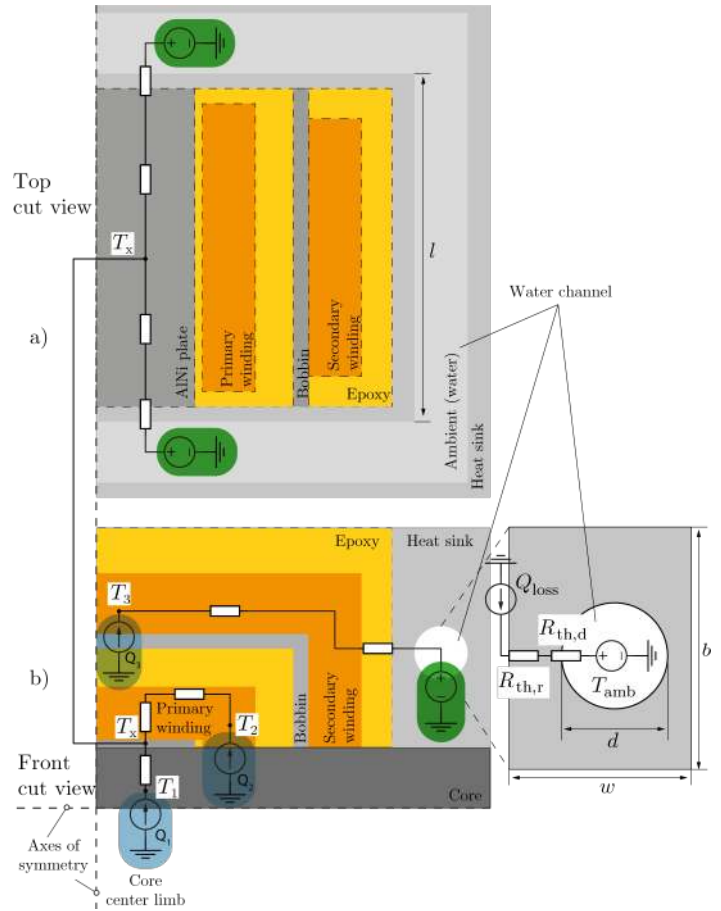


Figure 9. Simplified thermal model of the transformer with model of the channel. The shown thermal network is a reduction of the full scale model having 11 nodes and expressed as 11×11 size matrix.

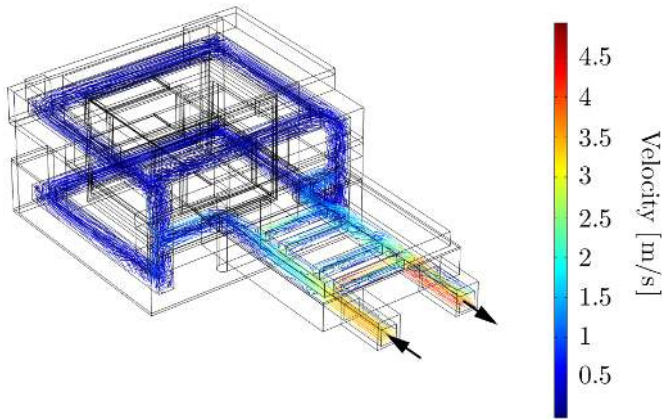


Figure 10. Water velocity field inside the presented converter cooling structure.

factor, can be used

$$f = \frac{64}{Re} \quad (17)$$

where $Re = V \cdot d/\nu$ is the *Reynolds* number. Finally, the obtained fluid flow rate is then used in expression eq. (10) in order to calculate the thermal resistance of the water channel (eqs. (6) and (7)). For the channels which have a turbulent flow, *Haaland's* equation offers good approximation of the turbulent region of the *Moody* chart [28]

$$f = \left[-1.8 \log \left[\frac{6.9}{Re} + \frac{\epsilon/d^{1.11}}{3.7} \right] \right]^{-2} \quad (18)$$

where ϵ/d is the channel roughness ratio.

For designs with long channels and/or slow fluid flows, the temperature of the fluid can increase along the axial direction. In order to calculate this temperature rise of the fluid, an 1D energy balance expression [29] is used:

$$q'(x) = \dot{V} \rho C_p (T(x) - T_{in}) \quad (19)$$

where $q'(x) = q/x$ are the power losses per unit of length, ρ is the density of the fluid, C_p is the thermal capacity of fluid, and T_{in} , $T(x)$ are the input temperature and temperature at point x in axial direction, respectively.

III. FEM SIMULATIONS

In this section, results of FEM simulations are presented for different design aspects.

A. Leakage Inductance Simulation

For verifying the analytical model of the leakage inductance from section II-B, a 3D magnetic field simulation is performed. For the simulation, an 1 A current excitation of the primary and secondary windings are assumed with opposite directions, and the resulting total magnetic energy is obtained.

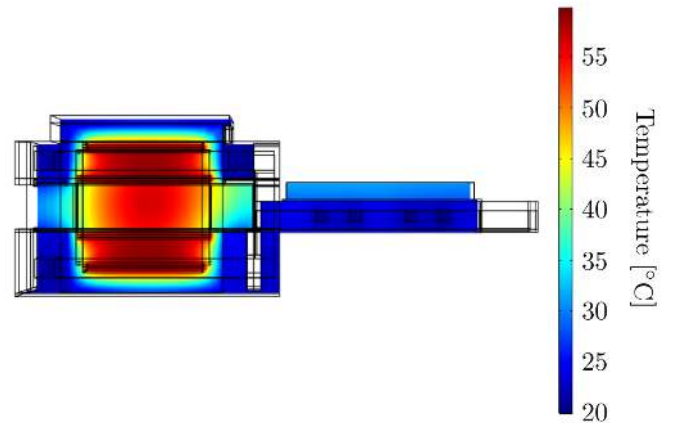


Figure 11. Temperature distribution of the integrated converter structure.

The leakage inductance is then calculated from the energy with

$$L_\sigma = \frac{2E_{tot}}{I^2} \quad (20)$$

The comparison of the calculated and simulated leakage inductance value is shown in table III.

Table III. COMPARISON BETWEEN THE VALUES OF THE LEAKAGE INDUCTANCE OBTAINED WITH THE ANALYTICAL CALCULATION AND THE 3D FEM SIMULATION.

	Analytical	FEM
Leakage inductance L_σ	26.5 μ H	26.2 μ H

B. Heat Transfer and CFD Simulations

In order to verify the thermal models presented in section II-C, combined 3D heat transfer and fluid dynamic FEM simulations were performed. The simulated velocity field inside the presented cooling structure is shown in fig. 10, while the temperature distribution is given in fig. 11. The input flow rate at the inlet is assumed to be 27 L/min and the inlet water temperature is equal to 20 °C, which corresponds to the flow rate and water temperature used during experimental measurement. The values of the material parameters for the analytical thermal calculations listed in table II are also used for the 3D FEM simulations. The comparison between the calculated temperatures of the transformer obtained with the presented thermal model from fig. 9 and the results from FEM simulations are given in table IV.

Table IV. CALCULATED TEMPERATURES OF THE TRANSFORMER WITH PRESENTED THERMAL MODEL (FIG. 9).

Temperature	Analytical	FEM
Core mid leg (T_1)	54 °C	56 °C
Primary winding (T_2)	56 °C	59 °C
Secondary winding (T_3)	59 °C	59 °C

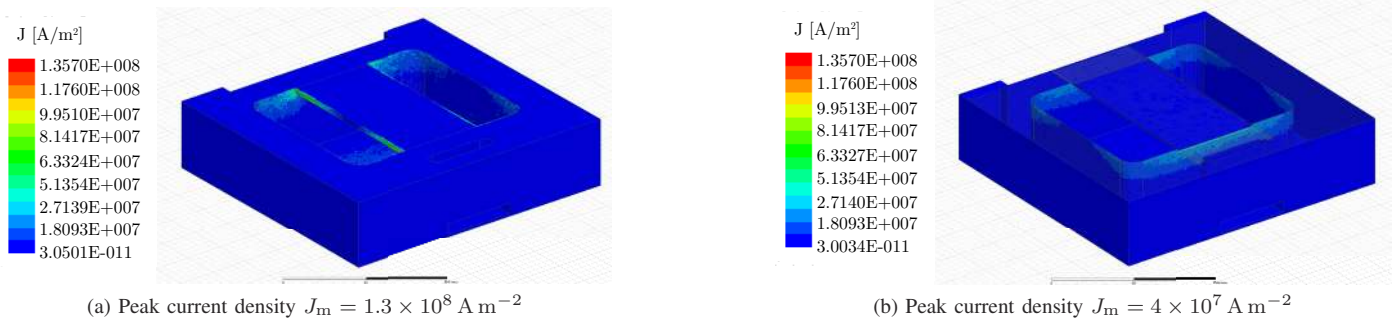


Figure 12. Eddy currents induced in the bottom cooling structure with a) Al bar and, b) AlNi bar, used for cooling of the primary transformer winding.

C. Eddy Current Simulations

In order to get the eddy current induced losses in the transformer cooling structure 3D FEM simulations were performed. There, two cases have been considered: 1) single Al bar located between the middle transformer leg and the primary winding on the bottom, 2) two AlNi bars located on top and bottom of the middle transformer leg. The surface current densities induced in the bottom cooling parts in case of the Al and AlNi bars are given in fig. 12. The peak current density with the AlNi bars is 3 times lower. The total losses induced in the transformer cooling structure for the two mentioned cases are given in table V.

Table V. INDUCED EDDY CURRENT LOSSES IN THE TRANSFORMER COOLING STRUCTURE.

	Al bar	AlNi bar
Induced losses	75 W	36 W

IV. EXPERIMENTAL RESULTS

A. Leakage Inductance Measurement

The leakage inductance is measured with the impedance analyzer, and the resulting short circuit inductance change with the frequency is depicted in fig. 13. Comparing the measurement results with the results of the analytical calculation and FEM simulation, given in table III, it can be seen that all match very well.

B. Thermal Measurement

In order to measure the temperature of the transformer winding, an NTC temperature probe is attached to the secondary winding prior to potting. For the thermal measurement the primary and secondary winding are supplied with constant DC currents. As a worst case approximation, the value of the supplied current is chosen such that the total transformer losses (core + winding losses), given in table II, are generated in the windings. The water cooling system was operated with constant flow rate of 27 L/min and a water temperature of 20 °C. In table VI, the measured secondary winding temperature is given, together with values obtained from analytical calculations and FEM simulations.

Table VI. SECONDARY WINDING TEMPERATURE MEASUREMENT RESULT.

Temperature	Analytical	FEM	Measured
Secondary winding	59 °C	59 °C	57 °C

C. Partial Discharge Measurement

The final measurement which have been performed is the partial discharge measurement. This measurement is performed by a 2.8 kV/50 Hz peak voltage to the secondary side winding while having the primary side winding and core grounded. The results of the partial discharge measurement procedure are depicted in fig. 14. As can be seen, the highest discharge values are lower than 18 pC, which can, for the given requirements, be regarded as partial discharge free.

V. CONCLUSION

In this paper, the design of a medium frequency transformer with integrated cooling structure is presented. The system integration with advanced cooling design results in a higher power density value (fig. 2). Detailed loss, leakage inductance and thermal models of the medium frequency transformer with integrated cooling structure are used to find the optimal design

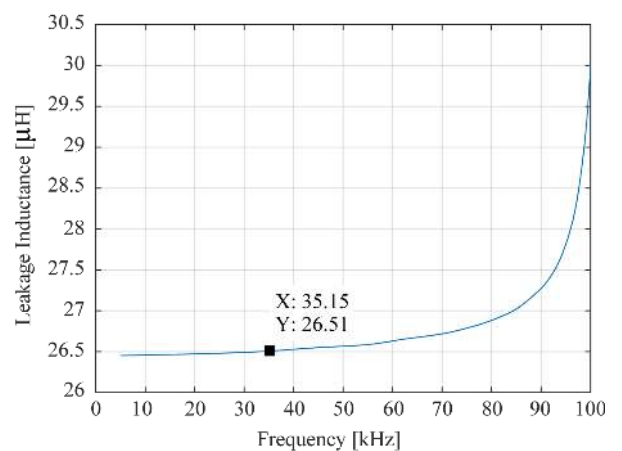


Figure 13. Measured short circuit inductance of the designed transformer. The nominal switching frequency is 35 kHz

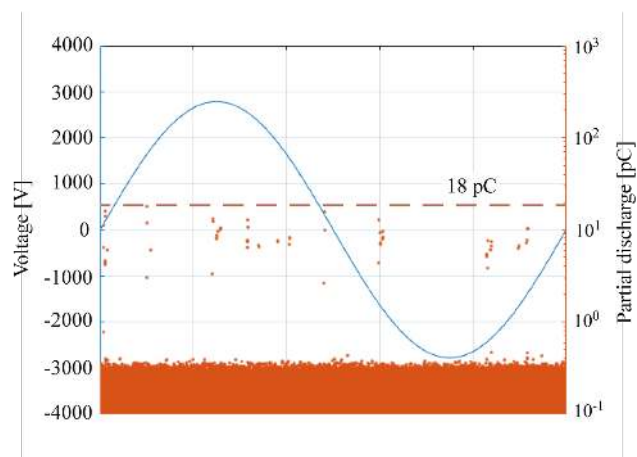


Figure 14. Results of the partial discharge measurement performed on the designed transformer. The figure shows the cumulative partial discharges during a testing period of 20 min, and their occurrence as a function of the supplied voltage.

parameters using the methodology presented in section II. The resulting design was validated with extensive FEM simulations for various design aspects. The final validation is performed with experimental measurements on the prototype system.

ACKNOWLEDGEMENT

This research is part of the activities of the Swiss Centre for Competence in Energy Research on Efficient Technologies and Systems for Mobility (SCCER Mobility), which is financially supported by the Swiss Innovation Agency (Innosuisse - SCCER program) and *Bombardier Transportation AG Switzerland*. CTI funding grant no.: PFIW-IW 18312.1

REFERENCES

- [1] "Uniflex-PM," 2009. [Online]. Available: http://www.eee.nott.ac.uk/uniflex/Documents/Deliverable%20D7_2_FINAL.pdf
- [2] G. Reed, G. Kusic, J. Svensson, and Z. Wang, "A case for medium voltage direct current (MVDC) power for distribution applications," in *IEEE-PES Power Systems Conference and Exposition*, 2011.
- [3] F. Mura and R. W. De Doncker, "Design aspects of a medium-voltage direct current (MVDC) grid for a university campus," in *IEEE 8th International Conference on Power Electronics and ECCE Asia*, 2011.
- [4] Y. Matsuoka, K. Takao, K. Wada, M. Nakahara, K. Sung, H. Ohashi, and S. Nishizawa, "2.5kV, 200kW bi-directional isolated DC/DC converter for medium-voltage applications," in *International Power Electronics Conference*, 2014.
- [5] M. Steiner and H. Reinold, "Medium frequency topology in railway applications," in *European Conf. on Power Electronics and Applications*, 2007.
- [6] J. Weigel, A. Ag, and H. Hoffmann, "High voltage IGBTs in medium frequency traction power supply," in *European Conference on Power Electronics and Applications*, 2009.
- [7] C. Zhao, S. Lewdeni-Schmid, J. Steinke, M. Weiss, T. Chaudhuri, M. Pellerin, J. Duron, and P. Stefanutti, "Design, implementation and performance of a modular power electronic transformer (PET) for railway application," in *European Conference on Power Electronics and Applications*, 2011.
- [8] G. Ortiz, "High-power DC-DC converter technologies for smart grid and traction applications," Ph.D. dissertation, ETH Zurich, 2014.
- [9] C. Chryssakis and B. J. Vartdal, "Ship electrification and alternative fuels," *Motorways of the Seas*, 2016.
- [10] A. Burke, "Batteries and ultracapacitors for electric, hybrid and fuel cell vehicles," in *Proceedings of the IEEE*, 2007.
- [11] S. Vasquez, S. Lukic, E. Galvan, L. Franquelo, and J. Carrasco, "Energy storage systems for transport and grid applications," *IEEE Trans. on Industrial Electronics*, 2010.
- [12] R. De Doncker, D. Divan, and M. Kheraluwala, "A three-phase soft-switched high power density DC-DC converter for high power applications," in *IEEE Industry Applications Society Annual Meeting*, 1988.
- [13] J. Biela, U. Badstubner, and J. Kolar, "Design of a 5kW, 1-U, 10kW/ltr. resonant DC-DC converter for telecom applications," in *29th International Telecommunications Energy Conference, INTELEC*, 2007.
- [14] K. W. Klontz, D. M. Divan, and D. W. Novotny, "An actively cooled 120 kW coaxial winding transformer for fast charging electric vehicles," *IEEE Trans. on Industry Applications*, 1995.
- [15] L. Heinemann, "An actively cooled high power, high frequency transformer with high insulation capability," in *IEEE Applied Power Electronics Conference and Exposition*, 2002.
- [16] H. Hoffmann and B. Piepenbreier, "Medium frequency transformer for rail application using new materials," in *1st International Electric Drives Production Conference*, 2011.
- [17] I. Villar, "Multiphysical characterization of medium-frequency power electronic transformers," Ph.D. dissertation, EPFL, Lausanne, 2010.
- [18] P. Shuai and J. Biela, "Design and optimization of medium frequency, medium voltage transformers," in *15th European Conference on Power Electronics and Applications*, 2013.
- [19] M. Mogorovic and D. Dujic, "Thermal modeling and experimental verification of an air cooled medium frequency transformer," in *19th European Conference on Power Electronics and Applications (EPE)*, 2017.
- [20] M. Pavlovsky, "Electronic dc transformer with high power density," Ph.D. dissertation, Technical University Delft, 2006.
- [21] M. A. Bahmani, "Design and optimization considerations of medium-frequency power transformers in high-power DC-DC applications," Ph.D. dissertation, Chalmers University of Technology, 2016.
- [22] M. Stojadinovic, E. Kalkounis, F. Jauch, and J. Biela, "Generalized PWM generator with transformer flux balancing for dual active bridge converter," in *Proc. 19th European Conf. Power Electronics and Applications (EPE)*, 2017.
- [23] M. H. Kheraluwala, D. Novotny, and D. M. Divan, "Coaxially wound transformers for high-power high-frequency applications," *IEEE Transactions on Power Electronics*, 1992.
- [24] E. Bennett and S. C. Larson, "Effective resistance to alternating currents of multilayer windings," *Transactions of the American Institute of Electrical Engineers*, 1940.
- [25] K. Venkatachalam, C. Sullivan, T. Abdallah, and H. Tacca, "Accurate prediction of ferrite core loss with nonsinusoidal waveforms using only steinmetz parameters," in *IEEE Workshop on Computers in Power Electronics*, 2002.
- [26] V. V. Kantor, "Methods of calculating leakage inductance of transformer windings," *Russian Electrical Engineering*, 2009.
- [27] Y. S. Muzychka, "Generalized models for laminar developing flows in heat sinks and heat exchangers," *Heat Transfer Engineering*, 2013.
- [28] F. M. White, *Fluid Mechanics*. McGraw-Hill, 1998.
- [29] S. Ghiaasiaan, *Convective Heat and Mass Transfer*. Cambridge University Press, 2011.